Prof. Yu Huang
State Key Lab of Loess and Quaternary Geology
Institute of Earth Environment, Chinese Academy of Sciences, Xi'an, 710061, China
Tel./Fax: (86) 29-62336261
E-mail: huangyu@ieecas.cn

Aug. 25, 2022

Dear Prof. Kourtchev,

Revision for Manuscript ACP-2022-376

We thank you very much for giving us the opportunity to revise our manuscript. We highly appreciate the reviewers for their comments and suggestions on the manuscript entitled "**Oligomer formation from the gas-phase reactions of Criegee intermediates with hydroperoxide esters: mechanism and kinetics**". We have made revisions of our manuscript carefully according to the comments and suggestions of reviewers. The revised contents are marked in blue color. The response letter to reviewers is attached at the end of this cover letter.

We hope that the revised manuscript can meet the requirement of Atmospheric Chemistry & Physics. Any further modifications or revisions, please do not hesitate to contact us.

Look forward to hearing from you as soon as possible.

Best regards,

Yu Huang

Comments of reviewer #3

1. For Entry 1 of the initiation reaction, how is it validated that 1,4 O-H insertion is barrierless? Is there a multi-point potential energy surface showing that no barrier is found along the reaction coordinate?

Response: Based on the Reviewer's suggestion, the relevance descriptions on the barrierless 1,4 O-H insertion reactions have been added in the revised manuscript. The potential energy surface (PES) of the initiation reactions of distinct stabilized Criegee intermediates (SCIs) (CH_2OO, *syn*-, *anti*-CH_3CHOO and $(CH_3)_2COO$) with HCOOH is drawn in Fig. 1. As shown in Fig. 1, the bimolecular reaction of distinct SCIs with HCOOH proceeds via four possible pathways, namely (1) 1,4 O-H insertion (Entry 1), (2) 1,2 O-H insertion (Entry 2), (3) C-H insertion (Entry 3), and (4) C=O cycloaddition (Entry 4). For Entry 1, the addition reaction of CH_2OO with HCOOH proceeds through the 1,4 O-H insertion of CH_2OO into HCOOH to form a hydroperoxide ester HC(O)O-CH_2OO-H with a exoergicity of 37.6 kcal·mol^{-1}. The formation of HC(O)O-CH_2OO-H is obtained through a concerted process of O_2-H_2 bond breaking in the HCOOH and O_4-H_2 and C_2-O_1 bonds forming. Despite an attempt by various methods, the corresponding transition state is still not located in the effort of optimization. To further validate the barrierless process of 1,4 O-H insertion reaction, a relaxed scan over the O_4-H_2 and C_2-O_1 bonds is performed at the M06-2X/6-311+G(2df,2p) level of theory. The scans start from the optimized structure of the adduct product HC(O)O-CH_2OO-H, and the O_4-H_2 and C_2-O_1 bond length are then increased in steps of 0.10 Å. The relaxed scan energy profiles are presented in Fig. S2. As seen in Fig. S2a, the relative energy of the minimum energy path from reactant to product decreases monotonically when the bond length of O_4-H_2 and C_2-O_1 bonds decreases, suggesting that the transition state is not exist in the 1,4 O-H insertion reaction of CH_2OO with HCOOH. Similar conclusion is also obtained from the relaxed scan energy profiles for the HCOOH + *anti*-CH_3CHOO, HCOOH + *syn*-CH_3CHOO and HCOOH + $(CH_3)_2COO$ (Fig. S2b-d) reactions that 1,4 O-H insertion reactions are barrierless. This conclusion is further supported by the analogous reaction systems that 1,4 O-H insertion reactions of carbonyl oxides with carboxylic acids are a barrierless process including concerted hydrogen atom transfer and new bond formation (Long et al., 2009; Vereecken, 2017; Cabezas and Endo, 2019; Lin et al., 2019; Chhantyal-Pun et al., 2017).

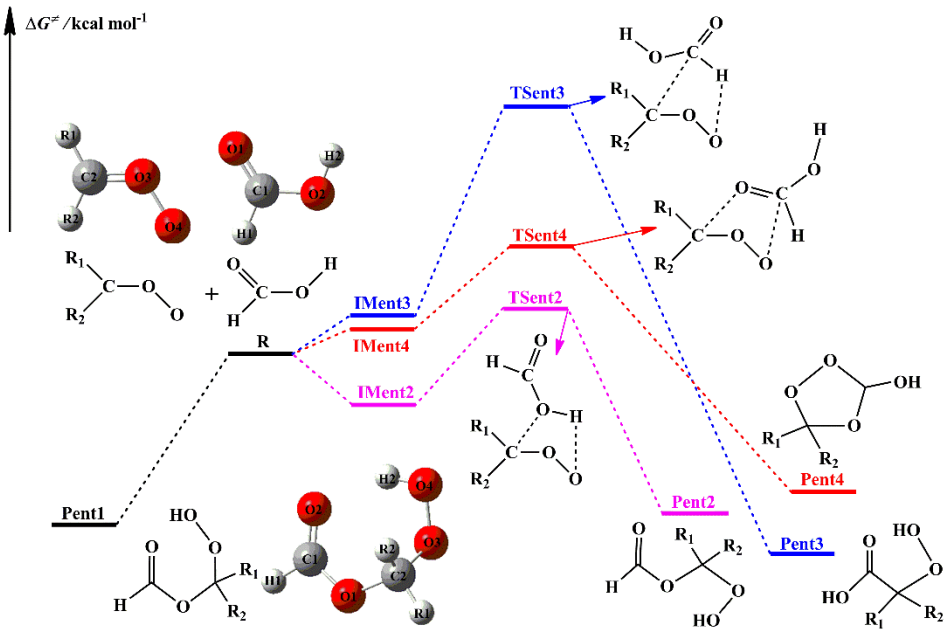

Figure 1. Schematic PES for the possible entrance pathways of the initiation reactions of HCOOH with various SCIs (black, pink, blue, and red lines represent 1,4 O-H insertion, 1,2 O-H insertion, C-H insertion, and C=O cycloaddition reactions, respectively)

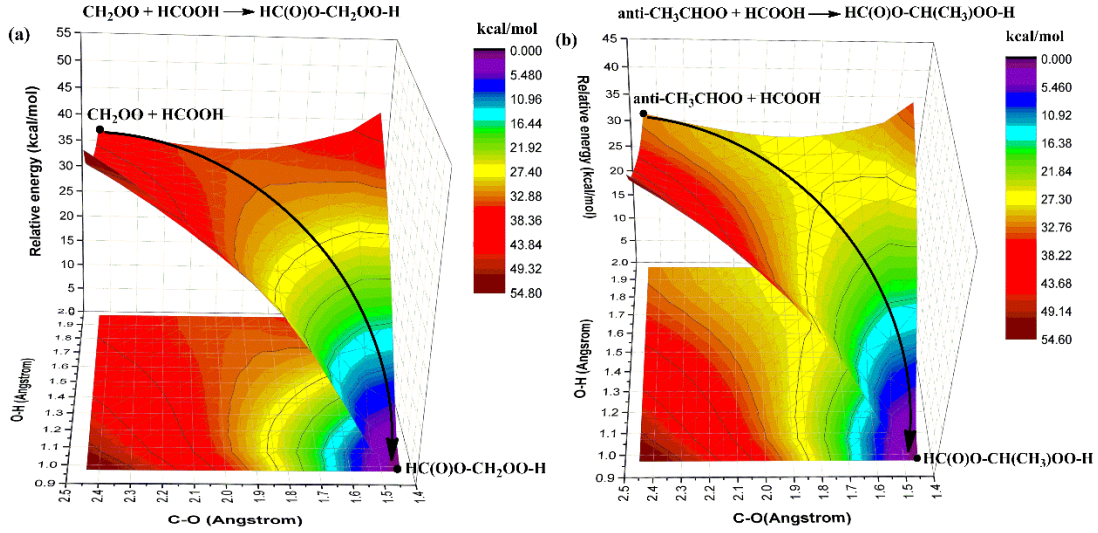

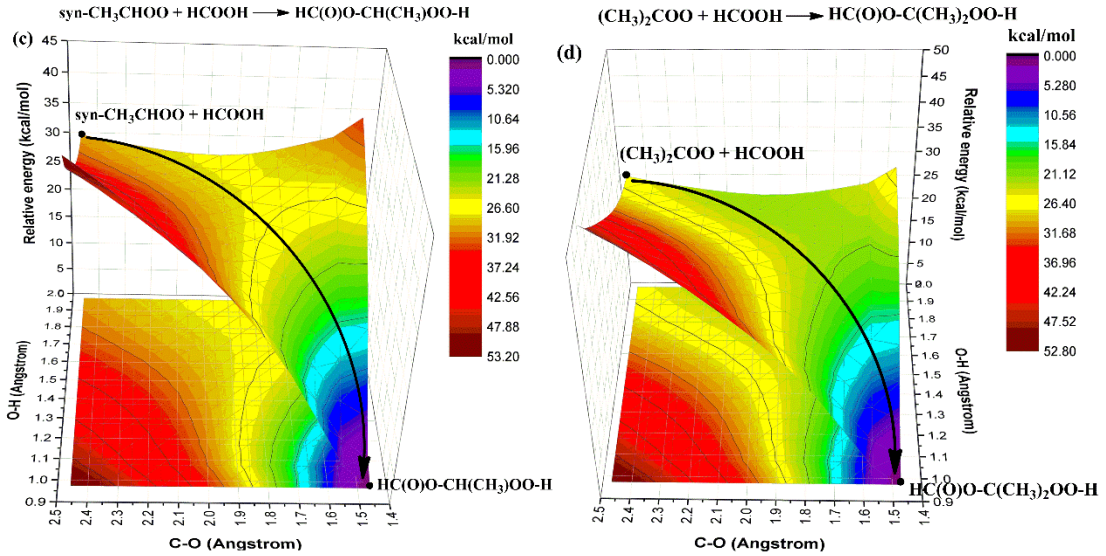

Figure S2. Relaxed scan energy profiles calculated using the M06-2X/6-311+G(2df,2p) method for varying the C-O and O-H bonds in the 1,4-insertion reactions CH_2OO + HCOOH (a), *anti*-CH_3CHOO + HCOOH (b), *syn*-CH_3CHOO + HCOOH (c) and $(CH_3)_2COO$ + HCOOH (d) (the black solid line represents the minimum energy path)

Corresponding descriptions have been added in the page 8 line 215-239 of the revised manuscript:

The potential energy surface (PES) of distinct SCIs (CH_2OO, syn-, anti-CH_3CHOO and $(CH_3)_2COO$) reactions with HCOOH is drawn in Fig. 1. As shown in Fig. 1, the bimolecular reaction of distinct SCIs with HCOOH proceeds via four possible pathways, namely (1) 1,4 O-H insertion (Entry 1), (2) 1,2 O-H insertion (Entry 2), (3) C-H insertion (Entry 3), and (4) C=O cycloaddition (Entry 4). For Entry 1, the addition reaction of CH_2OO with HCOOH proceeds through the 1,4 O-H insertion of CH_2OO into HCOOH to form a hydroperoxide ester HC(O)O-CH_2OO-H with a exoergicity of 37.6 kcal·mol^{-1}. The formation of HC(O)O-CH_2OO-H is obtained through a concerted process of O_2-H_2 bond breaking in the HCOOH and O_4-H_2 and C_2-O_1 bonds forming. Despite an attempt by various methods, the corresponding transition state is still not located in the effort of optimization. To further validate the barrierless process of 1,4 O-H insertion reaction, a relaxed scan over the O_4-H_2 and C_2-O_1 bonds is performed at the M06-2X/6-311+G(2df,2p) level of theory. The scans start from the optimized structure of the adduct product HC(O)O-CH_2OO-H, and the O_4-H_2 and C_2-O_1 bond length are then increased in steps of 0.10 Å. The relaxed scan energy profiles are presented in Fig. S2. As seen in Fig. S2a, the relative energy of the minimum energy path from reactant to product decreases monotonically when the bond length of O_4-H_2 and C_2-O_1 bonds decreases, suggesting that the transition state is not exist in the 1,4 O-H

insertion reaction of CH_2OO with HCOOH. Similar conclusion is also obtained from the relaxed scan energy profiles for the HCOOH + anti-CH_3CHOO, HCOOH + syn-CH_3CHOO and HCOOH + $(CH_3)_2COO$ (Fig. S2b-d) reactions that 1,4 O-H insertion reactions are barrierless. This conclusion is further supported by the analogous reaction systems that 1,4 O-H insertion reactions of carbonyl oxides with carboxylic acids are a barrierless process including concerted hydrogen atom transfer and new C-O bond formation (Chhantyal-Pun et al., 2017; Long et al., 2009; Vereecken, 2017; Cabezas and Endo, 2019; Lin et al., 2019).

2. The calculated k_{tot} in this study is greater by a factor of ~3 than several previous studies. Since this is related to one of the major conclusions of the paper, the authors should carefully validate this result. For example, what could be the reason they underestimate the value? Which value can have a better interpretation of the experimental or atmospheric data?

Response: In the original manuscript, the rate coefficients for the barrierless reactions are calculated by employing the variational transition state theory (VTST), and the rate coefficients for the bimolecular reactions with the tight transition states are computed by using the canonical transition state theory (CTST) along with one-dimensional asymmetric Eckart tunneling correction. For the initiation reactions of distinct SCIs with HCOOH, there are four possible pathways, namely (1) 1,4 O-H insertion (Entry 1), (2) 1,2 O-H insertion (Entry 2), (3) C-H insertion (Entry 3), and (4) C=O cycloaddition (Entry 4), in which Entry 1 is barrierless and Entry 2-4 have the tight transition states. The total rate coefficient for the reaction of SCIs with HCOOH is equal to the sum of the rate coefficient of each pathway. For the barrierless 1,4 O-H insertion reaction, the VTST is approximated with a Morse potential function, $V(\mathrm{R}) = D_e\{1\text{-}\exp[-\beta(R\text{-}R_e)]\}^2$, along with an anisotropy potential function to stand for the minimum energy path, which is used to calculate the rate coefficients (Raghunath et al., 2017). Here, D_e is the bond energy excluding the zero-point energy, R is the reaction coordinate, and R_e is the equilibrium value of R. It is assumed that the stretching potential in an anisotropy potential is used in conjunction with a potential form of $V_{anisotropy} = V_0[1\text{-}\cos^2(\theta_1\text{–}\theta_{1e}) \times \cos^2(\theta_2\text{–}\theta_{2e})]$ (Raghunath et al., 2017). Here, V_0 is the stretching potential, which stands for by a Morse potential, θ_1 and θ_{1e} represent the rotational angle between fragment 1 and the reference axis and the equilibrium bond angle of fragment 1, θ_2 and θ_{2e} stand for the rotational angle between fragment 2 and the reference axis and the equilibrium bond angle of

fragment 2. The association curve for the reaction of 1,4 O-H insertion of SCIs into HCOOH is computed at the M06-2X/6-311+G(2df,2p) level of theory to cover a range from 0.97 to 1.97 Å at step size 0.1 Å for O-H bond and from 1.44 to 2.44 Å at step size 0.1 Å for C-O bond, while other structural parameters are fully optimized. The computed potential energies are fitted to the Morse potential function. However, the calculated rate coefficients for the reactions of SCIs with HCOOH are higher than the prior experimental measurements. The reason is ascribed to the fact that the approximation of VTST using a Morse potential function in conjunction with an anisotropy potential function is unsuitable to predict the rate coefficients for the barrierless 1,4 O-H insertion reaction.

In the revised manuscript, the rate coefficients for the barrierless reactions are computed by employing the inverse Laplace transformation (ILT) method, and the rate coefficients for the bimolecular reactions with the tight transition states are calculated by utilizing CTST in conjunction with Eckart tunneling correction. The ILT and CTST/Eckart calculations are performed by using the MESMER 6.0 and KiSThelP 2019 programs, respectively (Glowacki et al., 2012; Canneaux et al., 2013). In the ILT treatment, the rotational constants, vibrational frequencies, molecular weights, energies and other input parameters are obtained from the M06-2X/6-311+G(2df,2p) or M06-2X/ma-TZVP methods. For the barrierless reaction of 1,4 O-H insertion of SCIs into HCOOH, SCIs and HCOOH are assigned as the deficient and excess reactants, respectively. The concentration of HCOOH is given a value of 5.0×10^{10} molecules cm^{-3} in the simulation, which is taken from the typical concentration of HCOOH in the tropical forest environments (Vereecken et al., 2012). N_2 is applied as the buffer gas. A single exponential down model is employed to simulate the collision transfer ($<\Delta E>_{down}$ = 200 cm^{-1}). The collisional Lennard-Jones parameters are estimated with the empirical formula described by Gilbert and Smith (1990).

The rate coefficients of each elementary pathway included in the initiation reactions of distinct SCIs with HCOOH are calculated in the temperature range of 273-400 K, as listed in Table S3-S6. As shown in Table S3, the total rate coefficients $k_{tot\text{-}CH2OO}$ of CH_2OO reaction with HCOOH are in excess of 1.0×10^{-10} cm^3 $molecule^{-1}$ s^{-1}, and they exhibit a slightly negative temperature dependence in the temperature range studied. $k_{tot\text{-}CH2OO}$ is estimated to be 1.4×10^{-10} cm^3 $molecule^{-1}$ s^{-1} at 298 K, which is in good agreement with the experimental values reported by Welz et al. (2014) ($[1.1 \pm 0.1] \times 10^{-10}$), Chung et al. (2019) ($[1.4 \pm 0.3] \times 10^{-10}$), and Peltola et al. (2020) ($[1.0 \pm 0.03] \times 10^{-10}$). $k(TS_{ent1})$ is approximately equal to $k_{tot\text{-}CH2OO}$ in the whole temperature range, and it decreases in the

range of 1.7×10^{-10} (273 K) to 1.2×10^{-10} (400 K) cm^3 $molecule^{-1}$ s^{-1} with increasing temperature. $k(TS_{ent1})$ is several orders of magnitude greater than $k(TS_{ent2})$, $k(TS_{ent3})$ and $k(TS_{ent4})$ over the temperature range from 273 to 400 K. The result again shows that the barrierless 1,4 O-H insertion reaction is predominant. Similar conclusion is also obtained from the results of the rate coefficients for the reactions of HCOOH with *anti*-CH_3CHOO, *syn*-CH_3CHOO and $(CH_3)_2COO$ (Table S4-S6). At ambient temperature, the total rate coefficients of HCOOH reactions with *anti*-CH_3CHOO, *syn*-CH_3CHOO and $(CH_3)_2COO$ are estimated to be 5.9, 2.7 and 4.8×10^{-10} cm^3 $molecule^{-1}$ s^{-1}, respectively, which are consistent with the prior experimental measurements of 5 ± 3, 2.5 ± 0.3 and 4.5×10^{-10} cm^3 $molecule^{-1}$ s^{-1} (Welz et al., 2014; Chung et al., 2019; Sipilä et al., 2014).

Table S3 Rate coefficients (cm^3 $molecule^{-1}$ s^{-1}) of each elementary pathway involved in the initiation reaction of CH_2OO with HCOOH computed at different temperatures

T/K	k (TS_{ent1})	k (TS_{ent2})	k (TS_{ent3})	k (TS_{ent4})	$k_{tot\text{-}CH2OO}$
273	1.7×10^{-10}	3.6×10^{-12}	1.0×10^{-22}	3.6×10^{-12}	1.8×10^{-10}
280	1.6×10^{-10}	2.9×10^{-12}	1.2×10^{-22}	3.1×10^{-12}	1.7×10^{-10}
298	1.4×10^{-10}	1.9×10^{-12}	2.2×10^{-22}	2.3×10^{-12}	1.4×10^{-10}
300	1.4×10^{-10}	1.8×10^{-12}	2.4×10^{-22}	2.2×10^{-12}	1.4×10^{-10}
320	1.3×10^{-10}	1.2×10^{-12}	4.9×10^{-22}	1.6×10^{-12}	1.3×10^{-10}
340	1.3×10^{-10}	8.2×10^{-13}	1.0×10^{-21}	1.3×10^{-12}	1.3×10^{-10}
360	1.2×10^{-10}	5.9×10^{-13}	2.2×10^{-21}	1.0×10^{-12}	1.2×10^{-10}
380	1.2×10^{-10}	4.5×10^{-13}	4.5×10^{-21}	8.2×10^{-13}	1.2×10^{-10}
400	1.2×10^{-10}	3.5×10^{-13}	9.0×10^{-21}	6.9×10^{-13}	1.2×10^{-10}

Table S4 Rate coefficients (cm^3 $molecule^{-1}$ s^{-1}) of each elementary pathway involved in the initiation reaction of *anti*-CH_3CHOO with HCOOH computed at different temperatures

T/K	k (TS_{ent1}-*anti*)	k (TS_{ent2}-*anti*)	k (TS_{ent3}-*anti*)	k (TS_{ent4}-*anti*)	$k_{tot\text{-}anti}$
273	5.9×10^{-10}	4.2×10^{-11}	5.5×10^{-22}	6.1×10^{-11}	6.9×10^{-10}
280	5.7×10^{-10}	3.8×10^{-11}	6.7×10^{-22}	4.9×10^{-11}	6.6×10^{-10}
298	5.4×10^{-10}	2.3×10^{-11}	1.2×10^{-21}	3.0×10^{-11}	5.9×10^{-10}
300	5.3×10^{-10}	2.0×10^{-11}	1.3×10^{-21}	2.8×10^{-11}	5.8×10^{-10}
320	5.0×10^{-10}	1.5×10^{-11}	2.6×10^{-21}	1.7×10^{-11}	5.3×10^{-10}
340	4.7×10^{-10}	9.4×10^{-12}	5.4×10^{-21}	1.1×10^{-11}	4.9×10^{-10}

360	4.5×10^{-10}	7.0×10^{-12}	1.1×10^{-20}	7.8×10^{-12}	4.7×10^{-10}
380	4.4×10^{-10}	3.6×10^{-12}	2.1×10^{-20}	5.6×10^{-12}	4.5×10^{-10}
400	4.3×10^{-10}	2.0×10^{-12}	4.0×10^{-20}	4.2×10^{-12}	4.4×10^{-10}

Table S5 Rate coefficients (cm^3 $molecule^{-1}$ s^{-1}) of each elementary pathway involved in the initiation reaction of *syn*-CH_3CHOO with HCOOH computed at different temperatures

T/K	k (TS_{ent1}-*syn*)	k (TS_{ent2}-*syn*)	k (TS_{ent3}-*syn*)	k (TS_{ent4}-*syn*)	$k_{tot\text{-}syn}$
273	3.1×10^{-10}	9.5×10^{-13}	4.6×10^{-27}	7.5×10^{-16}	3.1×10^{-10}
280	2.8×10^{-10}	8.0×10^{-13}	7.1×10^{-27}	6.4×10^{-16}	2.8×10^{-10}
298	2.7×10^{-10}	5.4×10^{-13}	8.9×10^{-26}	5.5×10^{-16}	2.7×10^{-10}
300	2.7×10^{-10}	5.2×10^{-13}	9.9×10^{-26}	4.6×10^{-16}	2.7×10^{-10}
320	2.5×10^{-10}	3.6×10^{-13}	3.0×10^{-25}	3.8×10^{-16}	2.5×10^{-10}
340	2.5×10^{-10}	2.6×10^{-13}	9.1×10^{-25}	3.1×10^{-16}	2.5×10^{-10}
360	2.3×10^{-10}	2.0×10^{-13}	2.6×10^{-24}	3.0×10^{-16}	2.3×10^{-10}
380	2.2×10^{-10}	1.5×10^{-13}	7.2×10^{-24}	2.4×10^{-16}	2.2×10^{-10}
400	2.2×10^{-10}	1.2×10^{-13}	1.8×10^{-23}	2.2×10^{-16}	2.2×10^{-10}

Table S6 Rate coefficients (cm^3 $molecule^{-1}$ s^{-1}) of each elementary pathway involved in the initiation reaction of $(CH_3)_2OO$ with HCOOH computed at different temperatures

T/K	k (TS_{ent1}-*dim*)	k (TS_{ent2}-*dim*)	k (TS_{ent3}-*dim*)	k (TS_{ent4}-*dim*)	$k_{tot\text{-}dim}$
273	5.3×10^{-10}	6.8×10^{-12}	1.4×10^{-26}	4.4×10^{-15}	5.4×10^{-10}
280	5.1×10^{-10}	5.2×10^{-12}	2.2×10^{-26}	4.2×10^{-15}	5.2×10^{-10}
298	4.8×10^{-10}	2.8×10^{-12}	8.0×10^{-26}	4.0×10^{-15}	4.8×10^{-10}
300	4.7×10^{-10}	2.6×10^{-12}	9.2×10^{-26}	3.9×10^{-15}	4.7×10^{-10}
320	4.5×10^{-10}	1.4×10^{-12}	3.6×10^{-25}	3.7×10^{-15}	4.5×10^{-10}
340	4.2×10^{-10}	8.6×10^{-13}	1.3×10^{-24}	3.6×10^{-15}	4.2×10^{-10}
360	3.9×10^{-10}	5.5×10^{-13}	4.5×10^{-24}	3.5×10^{-15}	3.9×10^{-10}
380	3.7×10^{-10}	3.7×10^{-13}	1.4×10^{-23}	3.4×10^{-15}	3.7×10^{-10}
400	3.7×10^{-10}	2.6×10^{-13}	3.9×10^{-23}	3.4×10^{-15}	3.7×10^{-10}

Corresponding descriptions have been added in the page 7 line 173-190, page 11 line 303-315, page 12 line 330-338 and page 13 line 346-351 of the revised manuscript:

The rate coefficients for the barrierless reactions are determined by employing the inverse Laplace transformation (ILT) method. The ILT calculations are performed with the MESMER 6.0 program (Glowacki et al., 2012). In the ILT treatment, the rotational constants, vibrational frequencies, molecular weights, energies and other input parameters are obtained from the M06-2X/6-311+G(2df,2p) or M06-2X/ma-TZVP methods. For the barrierless reaction of 1,4 O-H insertion of SCIs into HCOOH, SCIs and HCOOH are assigned as the deficient and excess reactants, respectively. The concentration of HCOOH is given a value of 5.0 × 10^{10} molecules cm^{-3} in the simulation, which is taken from the typical concentration of HCOOH in the tropical forest environments (Vereecken et al., 2012). N_2 is applied as the buffer gas. A single exponential down model is employed to simulate the collision transfer ($<\Delta E>_{down}$ = 200 cm^{-1}). The collisional Lennard-Jones parameters are estimated with the empirical formula described by Gilbert and Smith (1990).

The rate coefficients for the bimolecular reactions with the tight transition states are calculated by using the canonical transition state theory (CTST) along with one-dimensional asymmetric Eckart tunneling correction (Truhlar et al., 1996; Eckart, 1930). The CTST/Eckart calculations are performed with the KiSThelP 2019 program (Canneaux et al., 2013).

The rate coefficients of each elementary pathway included in the initiation reactions of distinct SCIs with HCOOH are calculated in the temperature range of 273-400 K, as listed in Table S3-S6. As shown in Table S3, the total rate coefficients $k_{tot\text{-}CH2OO}$ of CH_2OO reaction with HCOOH are in excess of 1.0 × 10^{-10} cm^3 $molecule^{-1}$ s^{-1}, and they exhibit a slightly negative temperature dependence in the temperature range studied. $k_{tot\text{-}CH2OO}$ is estimated to be 1.4 × 10^{-10} cm^3 $molecule^{-1}$ s^{-1} at 298 K, which is in good agreement with the experimental values reported by Welz et al. (2014) ([1.1 ± 0.1] × 10^{-10}), Chung et al. (2019) ([1.4 ± 0.3] × 10^{-10}), and Peltola et al. (2020) ([1.0 ± 0.03] × 10^{-10}). $k(TS_{ent1})$ is approximately equal to $k_{tot\text{-}CH2OO}$ in the whole temperature range, and it decreases in the range of 1.7 × 10^{-10} (273 K) to 1.2 × 10^{-10} (400 K) cm^3 $molecule^{-1}$ s^{-1} with increasing temperature. $k(TS_{ent1})$ is several orders of magnitude greater than $k(TS_{ent2})$, $k(TS_{ent3})$ and $k(TS_{ent4})$ over the temperature range from 273 to 400 K. The result again shows that the barrierless 1,4 O-H insertion reaction is predominant.

Equivalent to the case of CH_2OO reaction with HCOOH, the rate coefficient of each elementary pathway involved in the anti-CH_3CHOO + HCOOH reaction also decreases with the

temperature increasing (Table S4). This table shows that Entry 1 is kinetically favored over Entry 2, 3 and 4, and Entry 2 is competitive with Entry 4 in the range 273-400 K. Similar conclusion is also obtained from the results of the rate coefficients for the reactions of syn-CH_3CHOO and $(CH_3)_2COO$ with HCOOH that Entry 1 is the dominant pathway (Table S5-S6). It deserves mentioning that the competition of Entry 2 is significantly greater than that of Entry 4 in the syn-CH_3CHOO + HCOOH and $(CH_3)_2COO$ + HCOOH systems. At ambient temperature, the total rate coefficients of HCOOH reactions with anti-CH_3CHOO, syn-CH_3CHOO and $(CH_3)_2COO$ are estimated to be 5.9, 2.7 and 4.8 × 10^{-10} cm^3 $molecule^{-1}$ s^{-1}, respectively, which are consistent with the prior experimental measurements of 5 ± 3, 2.5 ± 0.3 and 4.5 × 10^{-10} cm^3 $molecule^{-1}$ s^{-1} (Welz et al., 2014; Chung et al., 2019; Sipilä et al., 2014).

3. Why are $k(TS_{ent2})$ and $k(TS_{ent4})$ decrease with increasing temperature as they both have positive energy barrier? (Table S3)

Response: Based on the Reviewer's suggestion, the relevance descriptions on the negative temperature dependence of $k(TS_{ent2})$ and $k(TS_{ent4})$ in Table S3 have been added in the revised manuscript. The rate coefficients for the bimolecular reactions with the tight transition states are calculated by using the canonical transition state theory (CTST) along with one-dimensional asymmetric Eckart tunneling correction. The initiation reaction of CH_2OO with HCOOH proceeds through four possible pathways, namely (1) 1,4 O-H insertion (Entry 1), (2) 1,2 O-H insertion (Entry 2), (3) C-H insertion (Entry 3), and (4) C=O cycloaddition (Entry 4). A schematic PES for the possible entrance pathways is drawn in Fig. 1. As shown in Fig. 1, the entrance pathway Entry2 consists of two elementary steps: (i) an intermediate IMent2 is formed via a barrierless process; (ii) then, it rearranges to the product Pent2 through a tight transition state TSent2. The whole reaction process can be described as Eq. (1):

$$CH_2OO + HCOOH \underset{k_{-1}}{\overset{k_1}{\rightleftarrows}} IMent2 \xrightarrow{k_2} Pent2 \quad (1)$$

Assuming the rapid equilibrium is established between the IMent2 and reactants. According to the steady-state approximation (SSA), the total rate coefficient is approximately expressed as Eq. (2):

$$k_{tot} = \frac{k_1}{k_{-1} + k_2} k_2 \approx \frac{k_1}{k_{-1}} k_2 = K_{eq} k_2 \quad (2)$$

The equilibrium constant K_{eq} is written as Eq. (3):

$$K_{eq} = \sigma \frac{Q_{IM}(T)}{Q_{R1}(T) Q_{R2}(T)} \exp\left(\frac{G_R - G_{IM}}{RT}\right) \quad (3)$$

where σ refers to the reaction symmetry number, $Q_{IM}(T)$, $Q_{R1}(T)$ and $Q_{R2}(T)$ denote the partition functions of intermediate, reactants R1 and R2, which are equal to the multiplication of translational, rotational, vibrational and electronic partition functions ($Q = Q_{rot}Q_{vib}Q_{trans}Q_{elec}$). T is the temperature in Kelvin, R is the ideal gas constant, G_R and G_{IM} are the total Gibbs free energies of reactant and intermediate, respectively. Similar methodology is adopted to calculate the rate coefficient of each elementary pathway in Entry 4.

The calculated $K_{eq\text{-}ent2}$, $k_{2\text{-}ent2}$, and $k(TS_{ent2})$ ($k(TS_{ent2}) = K_{eq\text{-}ent2} \times k_{2\text{-}ent2}$) in Entry 2 are listed in Table S7. This table shows that $K_{eq\text{-}ent2}$ significantly decreases with increasing temperature, and $k_{2\text{-}ent2}$ increases as the temperature is increased. However, the decreased value in $K_{eq\text{-}ent2}$ is greater than the increased value in $k_{2\text{-}ent2}$ under the same temperature range. For example, $K_{eq\text{-}ent2}$ deceases by a factor of 6.3 and $k_{2\text{-}ent2}$ increases by a factor of 2.9 at 298 K compared with the values of $K_{eq\text{-}ent2}$ and $k_{2\text{-}ent2}$ at 273 K. It is therefore that $k(TS_{ent2})$ decreases with the temperature increasing. Similar conclusion is also obtained from the results of the rate coefficients in Entry 4 that $k(TS_{ent4})$ exhibits a negative temperature dependence in the temperature range studied (Table S8). The aforementioned results imply that $k(TS_{ent2})$ and $k(TS_{ent4})$ are mediated by the pre-reactive complexes IMent2 and IMent4 in the Entry 2 and 4 of the CH_2OO + HCOOH reaction.

Table S7 $K_{eq\text{-}ent2}$ (cm^3 $molecule^{-1}$), $k_{2\text{-}ent2}$ (s^{-1}) and $k(TS_{ent2})$ (cm^3 $molecule^{-1}$ s^{-1}) in Entry 2 computed at different temperatures

T/K	$K_{eq\text{-}ent2}$	$k_{2\text{-}ent2}$	$k(TS_{ent2})$
273	8.2×10^{-17}	4.4×10^{4}	3.6×10^{-12}
280	4.7×10^{-17}	6.3×10^{4}	2.9×10^{-12}
298	1.3×10^{-17}	1.5×10^{5}	1.9×10^{-12}
300	1.1×10^{-17}	1.6×10^{5}	1.8×10^{-12}
320	3.2×10^{-18}	3.7×10^{5}	1.2×10^{-12}
340	1.1×10^{-18}	7.6×10^{5}	8.2×10^{-13}

360	4.1×10^{-19}	1.5×10^{6}	5.9×10^{-13}
380	1.7×10^{-19}	2.6×10^{6}	4.5×10^{-13}
400	8.0×10^{-20}	4.4×10^{6}	3.5×10^{-13}

Table S8 $K_{eq\text{-}ent4}$ (cm^3 $molecule^{-1}$), $k_{2\text{-}ent4}$ (s^{-1}) and $k(TS_{ent4})$ (cm^3 $molecule^{-1}$ s^{-1}) in Entry 4 computed at different temperatures

T/K	$K_{eq\text{-}ent4}$	$k_{2\text{-}ent4}$	$k(TS_{ent4})$
273	6.3×10^{-20}	5.7×10^{7}	3.6×10^{-12}
280	4.5×10^{-20}	7.0×10^{7}	3.1×10^{-12}
298	2.0×10^{-20}	1.1×10^{8}	2.3×10^{-12}
300	1.8×10^{-20}	1.2×10^{8}	2.2×10^{-12}
320	8.4×10^{-21}	1.9×10^{8}	1.6×10^{-12}
340	4.3×10^{-21}	2.9×10^{8}	1.3×10^{-12}
360	2.4×10^{-21}	4.2×10^{8}	1.0×10^{-12}
380	1.4×10^{-21}	5.9×10^{8}	8.2×10^{-13}
400	8.8×10^{-22}	7.9×10^{8}	6.9×10^{-13}

Corresponding descriptions have been added in the page 7 line 186-206 and page 12 line 315-326 of the revised manuscript:

The rate coefficients for the bimolecular reactions with the tight transition states are calculated by using the canonical transition state theory (CTST) along with one-dimensional asymmetric Eckart tunneling correction (Truhlar et al., 1996; Eckart, 1930). The CTST/Eckart calculations are performed with the KiSThelP 2019 program (Canneaux et al., 2013). As shown in Fig. 1, the entrance pathway Entry2 of R_1R_2COO reaction with HCOOH consists of two steps: (i) an intermediate IMent2 is formed via a barrierless process; (ii) then, it rearranges to the product Pent2 through a tight transition state TSent2. The whole reaction process can be described as Eq. (1):

$$R_1R_2COO + HCOOH \underset{k_{-1}}{\overset{k_1}{\rightleftharpoons}} IMent2 \xrightarrow{k_2} Pent2 \qquad (1)$$

Assuming the rapid equilibrium is established between the IMent2 and reactants. According to the steady-state approximation (SSA), the total rate coefficient is approximately expressed as Eq. (2) (Zhang et al., 2012):

$$k_{tot} = \frac{k_1}{k_{-1} + k_2} k_2 \approx \frac{k_1}{k_{-1}} k_2 = K_{eq} k_2 \quad (2)$$

The equilibrium constant K_{eq} is written as Eq. (3):

$$K_{eq} = \sigma \frac{Q_{IM}(T)}{Q_{R1}(T) Q_{R2}(T)} \exp\left(\frac{G_R - G_{IM}}{RT}\right) \quad (3)$$

where σ refers to reaction symmetry number, $Q_{IM}(T)$, $Q_{R1}(T)$ and $Q_{R2}(T)$ denote the partition functions of intermediate, reactants R1 and R2, which are equal to the multiplication of translational, rotational, vibrational and electronic partition functions ($Q = Q_{rot}Q_{vib}Q_{trans}Q_{elec}$) (Mendes et al., 2014), T is the temperature in Kelvin, R is the ideal gas constant, G_R and G_{IM} are the total Gibbs free energies of reactant and intermediate, respectively.

The calculated $K_{eq\text{-}ent2}$, $k_{2\text{-}ent2}$, and $k(TS_{ent2})$ ($k(TS_{ent2}) = K_{eq\text{-}ent2} \times k_{2\text{-}ent2}$) in Entry 2 are listed in Table S7. This table shows that $K_{eq\text{-}ent2}$ significantly decreases with increasing temperature, and $k_{2\text{-}ent2}$ increases as the temperature is increased. However, the decreased value in $K_{eq\text{-}ent2}$ is greater than the increased value in $k_{2\text{-}ent2}$ under the same temperature range. For example, $K_{eq\text{-}ent2}$ deceases by a factor of 6.3 and $k_{2\text{-}ent2}$ increases by a factor of 2.9 at 298 K compared with the values of $K_{eq\text{-}ent2}$ and $k_{2\text{-}ent2}$ at 273 K. It is therefore that $k(TS_{ent2})$ decreases with the temperature increasing. Similar conclusion is also obtained from the results of the rate coefficients in Entry 4 that $k(TS_{ent4})$ exhibits a negative temperature dependence in the temperature range studied (Table S8). The aforementioned results imply that $k(TS_{ent2})$ and $k(TS_{ent4})$ are mediated by the pre-reactive complexes IMent2 and IMent4 in the Entry 2 and 4.

4. The oligomerization reactions are highly dependent on the concentration of the monomers. Here the monomer are highly reactive SCIs and usually has very low concentration in the atmosphere. It seems that the high exothermicity of the oligomerization reaction results from the "stabilization" of SCIs in oligomerization. Also, the calculated free energies represent standard condition. Could the authors correct the Gibbs free energies by incorporating the atmospheric concentrations of SCIs (i.e., RTln(P/Pref)) to check whether this oligomerization is favored in the atmospheric conditions?

Response: Based on the Reviewer's suggestion, the relative importance of distinct SCIs reactions with hydroperoxide esters and trace species (e.g., H_2O, HCOOH and SO_2) has been added in the revised manuscript. It is well known that the reactions with trace species are expected to be

the dominant chemical sinks for SCIs in the atmosphere (Taatjes et al., 2013; Long et al., 2016). In the present study, the hydroperoxymethyl formate (HPMF) is selected as the model compound since it is the simplest hydroperoxide ester formed from the barrierless reaction of 1,4 O-H insertion of CH_2OO into HCOOH. The reported concentrations of coreactant, the rate coefficients k, and the effective pseudo-first-order rate constants ($k_{eff} = k$[coreactant]) for distinct SCI reactions with H_2O, HCOOH, SO_2, and HPMF are summarized in Table 2. As seen in Table 2, the rate coefficient of a particular SCI reaction with trace species is strongly dependent on its structure. The methyl group substitution may alter the rate coefficient by several to tens of times. The atmosphereric concentrations of H_2O, HCOOH and SO_2 in the tropical forest environments are measured to be 3.9-6.1 × 10^{17}, 5.0-10 × 10^{10}, and 1.7-9.0 × 10^{10} molecules cm^{-3}, respectively (Vereecken et al., 2012). For the reactions of CH_2OO with H_2O, HCOOH, and SO_2, the experimental rate coefficients are determined to be < 1.5 × 10^{-15}, [1.1 ± 0.1] × 10^{-10}, and [3.9 ± 0.7] × 10^{-11} cm^3 $molecule^{-1}$ s^{-1}, respectively (Welz et al, 2012 and 2014; Chao et al., 2015), which translate into $k_{eff(CH2OO+H2O)}$, $k_{eff(CH2OO+HCOOH)}$ and $k_{eff(CH2OO+SO2)}$ of 5.9-9.2 × 10^2, 5.5-11, and 0.7-3.5 s^{-1}, respectively. The result reveals that the reaction of CH_2OO with H_2O is the most important bimolecular reaction. $k_{eff(CH2OO+HCOOH)}$ is greater by a factor of 3-8 than $k_{eff(CH2OO+SO2)}$, indicating that the reaction of CH_2OO with HCOOH is favored over reaction with SO_2. Similar conclusion is also obtained from the results of k_{eff} for the reactions of *anti*-CH_3CHOO, *syn*-CH_3CHOO and $(CH_3)_2COO$ with H_2O, HCOOH and SO_2 that SCIs reactions with H_2O are faster than with HCOOH, which, in turn, are faster than with SO_2.

According to the results shown in the Table 2, the room temperature rate coefficient for the reaction of CH_2OO with HPMF is calculated to be 2.7 × 10^{-11} cm^3 $molecule^{-1}$ s^{-1}. However, to the best of our knowledge, the atmospheric concentration of HPMF has not been reported up to now. If we assume that the concentration of HPMF is the same as that of HCOOH, $k_{eff(CH2OO+HPMF)}$ is estimated to be 1.4-2.7 s^{-1}, which is significantly lower than $k_{eff(CH2OO+H2O)}$ and $k_{eff(CH2OO+HCOOH)}$. $k_{eff(CH2OO+HPMF)}$ is nearly identical to $k_{eff(CH2OO+SO2)}$, indicating that the CH_2OO + HPMF reaction is competitive with the CH_2OO + SO_2 system. Previous model-measurement studies have estimated the surface-level SCIs concentrations in the range of 1.0 × 10^4 to 1.0 × 10^5 molecules cm^{-3} (Khan et al., 2018; Novelli et al., 2017). If we assume that the concentration of HPMF is equal to that of SCIs, $k_{eff(CH2OO+HPMF)}$ is calculated to be 2.7-27 × 10^{-7} s^{-1}, which is several orders of magnitude lower than

$k_{eff(CH2OO+H2O)}$, $k_{eff(CH2OO+HCOOH)}$ and $k_{eff(CH2OO+SO2)}$. This result indicates that the reaction of CH_2OO with HPMF is of less importance. Similar conclusion is also obtained from the reactions of *anti*-CH_3CHOO, *syn*-CH_3CHOO and $(CH_3)_2COO$ with HPMF. Based on the above discussions, it can be concluded that the relative importance of carbonyl oxides reactions with hydroperoxide esters is significantly dependent on the concentrations of hydroperoxide esters. These reactions may play a certain role in the formation of organic new particle in some regions where low concentration of water vapour and high concentration of hydroperoxide esters occur.

Table 2 The reported concentrations of coreactant, the rate coefficients k, and the effective pseudo-first-order rate constants ($k_{eff} = k$[coreactant]) for distinct SCI reactions with HPMF, H_2O, HCOOH and SO_2 at the tropical forest environments

SCIs	Coreactant	[Coreactant] (molecules cm^{-3})	k (cm^3 $molecule^{-1}$ s^{-1})	k_{eff} (s^{-1})	Reference
CH_2OO	H_2O	$3.9\text{-}6.1 \times 10^{17}$	$< 1.5 \times 10^{-15}$	$5.9\text{-}9.2 \times 10^2$	Chao et al., (2015)
	HCOOH	$5.0\text{-}10.0 \times 10^{10}$	$[1.1 \pm 0.1] \times 10^{-10}$	5.5-11	Welz et al., (2014)
	SO_2	$1.7\text{-}9.0 \times 10^{10}$	$[3.9 \pm 0.7] \times 10^{-11}$	0.7-3.5	Welz et al., (2012)
	HPMF	-	2.7×10^{-11}	-	This work
anti-CH_3CHOO	H_2O	$3.9\text{-}6.1 \times 10^{17}$	$[1.0 \pm 0.4] \times 10^{-14}$	$3.9\text{-}6.1 \times 10^3$	Taatjes et al., (2013)
	HCOOH	$5.0\text{-}10.0 \times 10^{10}$	$[5 \pm 3] \times 10^{-10}$	25.0-50.0	Welz et al., (2014)
	SO_2	$1.7\text{-}9.0 \times 10^{10}$	$[6.7 \pm 1.0] \times 10^{-11}$	1.1-6.0	Taatjes et al., (2013)
	HPMF	-	3.3×10^{-10}	-	This work
syn-CH_3CHOO	H_2O	$3.9\text{-}6.1 \times 10^{17}$	$< 4.0 \times 10^{-15}$	$1.6\text{-}2.4 \times 10^3$	Taatjes et al., (2013)
	HCOOH	$5.0\text{-}10.0 \times 10^{10}$	$[2.5 \pm 0.3] \times 10^{-10}$	12.5-25.0	Welz et al., (2014)
	SO_2	$1.7\text{-}9.0 \times 10^{10}$	$[2.4 \pm 0.3] \times 10^{-11}$	0.4-2.2	Taatjes et al., (2013)
	HPMF	-	1.7×10^{-13}	-	This work
$(CH_3)_2COO$	H_2O	$3.9\text{-}6.1 \times 10^{17}$	$< 1.5 \times 10^{-16}$	58.5-91.5	Huang et al., (2015)
	HCOOH	$5.0\text{-}10.0 \times 10^{10}$	4.5×10^{-10}	22.5-45.0	Sipilä et al., (2014)

	SO_2	1.7-9.0 × 10^{10}	1.3 × 10^{-10}	2.2-11.7	Huang et al., (2015)
	HPMF	-	2.2 × 10^{-11}	-	This work

Corresponding descriptions have been added in the page 23 line 573-590 and page 24 line 591-610 of the revised manuscript:

It is of interest to assess whether the reactions of distinct SCIs with HPMF can compete well with the losses to reactions with trace species (e.g., H_2O, HCOOH and SO_2), because it is well known that the reactions with trace species are expected to be the dominant chemical sinks for SCIs in the atmosphere (Taatjes et al., 2013; Long et al., 2016). The reported concentrations of coreactant, the rate coefficients k, and the effective pseudo-first-order rate constants (k_{eff} = k[coreactant]) for distinct SCI reactions with H_2O, HCOOH, SO_2, and HPMF are summarized in Table 2. As seen in Table 2, the rate coefficient of a particular SCI reaction with trace species is strongly dependent on its structure. The methyl group substitution may alter the rate coefficient by several to tens of times. The atmospheric concentrations of H_2O, HCOOH and SO_2 in the tropical forest environments are measured to be 3.9-6.1 × 10^{17}, 5.0-10 × 10^{10}, and 1.7-9.0 × 10^{10} molecules cm^{-3}, respectively (Vereecken, 2012). For the reactions of CH_2OO with H_2O, HCOOH, and SO_2, the experimental rate coefficients are determined to be < 1.5 × 10^{-15}, [1.1 ± 0.1] × 10^{-10}, and [3.9 ± 0.7] × 10^{-11} cm^3 $molecule^{-1}$ s^{-1}, respectively (Welz et al., 2012 and 2014; Chao et al., 2015), which translate into $k_{eff(CH2OO+H2O)}$, $k_{eff(CH2OO+HCOOH)}$ and $k_{eff(CH2OO+SO2)}$ of 5.9-9.2 × 10^2, 5.5-11, and 0.7-3.5 s^{-1}, respectively. The result reveals that the reaction of CH_2OO with H_2O is the most important bimolecular reaction. $k_{eff(CH2OO+HCOOH)}$ is greater by a factor of 3-8 than $k_{eff(CH2OO+SO2)}$, indicating that the reaction of CH_2OO with HCOOH is favored over reaction with SO_2. Similar conclusion is also obtained from the results of k_{eff} for the reactions of anti-CH_3CHOO, syn-CH_3CHOO and $(CH_3)_2COO$ with H_2O, HCOOH and SO_2 that SCIs reactions with H_2O are faster than with HCOOH, which, in turn, are faster than with SO_2.

According to the results shown in the Table 2, the room temperature rate coefficient for the reaction of CH_2OO with HPMF is calculated to be 2.7 × 10^{-11} cm^3 $molecule^{-1}$ s^{-1}. However, to the best of our knowledge, the atmospheric concentration of HPMF has not been reported up to now. If we assume that the concentration of HPMF is the same as that of HCOOH, $k_{eff(CH2OO+HPMF)}$ is

estimated to be 1.4-2.7 s^{-1}, which is significantly lower than $k_{eff(CH2OO+H2O)}$ and $k_{eff(CH2OO+HCOOH)}$. $k_{eff(CH2OO+HPMF)}$ is nearly identical to $k_{eff(CH2OO+SO2)}$, indicating that the CH_2OO + HPMF reaction is competitive with the CH_2OO + SO_2 system. Previous model-measurement studies have estimated the surface-level SCIs concentrations in the range of 1.0 × 10^4 to 1.0 × 10^5 molecules cm^{-3} (Khan et al., 2018; Novelli et al., 2017). If we assume that the concentration of HPMF is equal to that of SCIs, $k_{eff(CH2OO+HPMF)}$ is calculated to be 2.7-27 × 10^{-7} s^{-1}, which is several orders of magnitude lower than $k_{eff(CH2OO+H2O)}$, $k_{eff(CH2OO+HCOOH)}$ and $k_{eff(CH2OO+SO2)}$. This result indicates that the reaction of CH_2OO with HPMF is of less importance. Similar conclusion is also obtained from the reactions of anti-CH_3CHOO, syn-CH_3CHOO and $(CH_3)_2COO$ with HPMF. Based on the above discussions, it can be concluded that the relative importance of carbonyl oxides reactions with hydroperoxide esters is significantly dependent on the concentrations of hydroperoxide esters. These reactions may play a certain role in the formation of organic new particle in some regions where low concentration of water vapour and high concentration of hydroperoxide esters occur.

5. Additionally, it would be helpful if there is some estimation about how much the oligomerization process could contribute to the regional or global SOA.

Response: Sakamoto et al. (2013) investigated the ozonolysis of ethylene in a Teflon bag reactor, and found that CH_2OO plays a critical role in the formations of oligomers and secondary organic aerosol (SOA) in the gas phase and particle phase. They proposed a possible formation mechanism for the oligomeric hydroperoxides, which includes the successive addition of CH_2OO to hydroperoxides. Sadezky et al. (2008) studied the gas-phase ozonolysis of small enol ethers in a 570 l spherical glass reactor at atmospheric conditions in the absence of seed aerosol. They found that the oligomers composed of Criegee intermediate as the repeated chain unit are the main constituents of SOA. Zhao et al. (2015) studied the ozonolysis of trans-3-hexene in both the static Teflon chamber and glass flow reactor under different relative humidity conditions. It was found that the oligomers having Criegee intermediate as the chain unit are the dominant components of SOA. These findings may help in understanding the potential pathway for the formation of SOA in the atmosphere. However, to the best of our knowledge, the contribution of the oligomerization reaction composed of Criegee intermediate as the chain unit to SOA remains unknown. In the future work, we will adopt the combination of quantum chemistry and numerical simulation to estimate

the contribution of oligomerization reaction to the regional and global SOA.

6. Line 39, “with increasing the number of SCIs” is a bit confusing, it would be better to say “with increasing the number of SCIs added to the oligomer”.

Response: The sentence “with increasing the number of SCIs” has been replaced by “with increasing the number of SCIs added to the oligomer” in the revised manuscript.

7. Line 491, “netative” should be “negative”.

Response: The word “netative” has been replaced by “negative” in the revised manuscript.

8. Line 499, “neartly” should be “nearly”.

Response: The word “neartly” has been replaced by “nearly” in the revised manuscript.

References

Cabezas, C., and Endo, Y.: The Criegee intermediate-formic acid reaction explored by rotational spectroscopy, Phys. Chem. Chem. Phys., 21, 18059-18064, https://doi.org/10.1039/c9cp03001h, 2019.

Canneaux, S., Bohr, F., and Henon, E.: KiSThelP: a program to predict thermodynamic properties and rate constants from quantum chemistry results, J. Comput. Chem., 35, 82-93, https://doi.org/10.1002/jcc.23470, 2013.

Chao, W., Hsieh, J. T., Chang, C. H., and Lin, J. J. M.: Direct kinetic measurement of the reaction of the simplest Criegee intermediate with water vapor, Science, 347, 751-754, https://doi.org/10.1126/science.1261549, 2015.

Chhantyal-Pun, R., McGillen, M. R., Beames, J. M., Khan, M. A. H., Percival, C. J., Shallcross, D. E., and Orr-Ewing, A. J.: Temperature Dependence of the Rates of Reaction of Trifluoracetic Acid with Criegee Intermediates, Angew. Chem. Int. Ed., 129, 9172-9175, https://doi.org/10.1002/anie.201703700, 2017.

Chung, C. A., Su, J. W., and Lee, Y. P.: Detailed mechanism and kinetics of the reaction of Criegee intermediate CH_2OO with HCOOH investigated via infrared identification of conformers of hydroperoxymethyl formate and formic acid anhydride, Phys. Chem. Chem. Phys., 21, 21445-21455, https://doi.org/10.1039/c9cp04168k, 2019.

Gilbert, R. G., and Smith, S. C.: Theory of unimolecular and recombination reactions; Blackwell Scientific: Carlton, Australia, 1990.

Glowacki, D. R., Liang, C. H., Morley, C., Pilling, M. J., and Robertson, S. H.: MESMER: an open-source master equation solver for multi-energy well reactions, J. Phys. Chem. A, 116, 9545-9560, https://doi.org/10.1021/jp3051033, 2012.

Huang, H. L., Chao, W., and Lin, J. J. M.: Kinetics of a Criegee intermediate that would survive high humidity and may oxidize atmospheric SO_2, Proc. Natl. Acad. Sci. U.S.A., 112, 10857-10862, https://doi.org/ 10.1073/pnas.1513149112, 2015.

Khan, M. A. H., Percival, C. J., Caravan, R. L., Taatjes, C. A., and Shallcross, D. E.: Criegee intermediates and their impacts on the troposphere, Environ. Sci.: Processes Impacts, 20, 437-453, https://doi.org/10.1039/C7EM00585G, 2018.

Lin, X., Meng, Q., Feng, B., Zhai, Y., Li, Y., Yu, Y., Li, Z., Shan, X., Liu, F., Zhang, L., and Sheng, L.: Theoretical study on Criegee intermediate's role in ozonolysis of acrylic acid, J. Phys. Chem. A, 123, 1929-1936, https://doi.org/10.1021/acs.jpca.8b11671, 2019.

Long, B., Bao, J. L., and Truhlar, D. G.: Atmospheric chemistry of Criegee intermediates: unimolecular reactions and reactions with water, J. Am. Chem. Soc., 138, 14409-14422, https://doi.org/10.1021/jacs.6b08655, 2016.

Long, B., Cheng, J. R., Tan, X. F., and Zhang, W. J.: Theoretical study on the detailed reaction mechanisms of carbonyl oxide with formic acid, J. Mol. Struc.: Theochem, 916, 159-167, https://doi.org/10.1016/j.theochem.2009.09.028, 2009.

Novelli, A., Hens, K., Ernest, C. T., Martinez, M., Nölscher, A. C., Sinha, V., Paasonen, P., Petäjä, T., Sipilä, M., Elste, T., Plass-Dülmer, C., Phillips, G. J., Kubistin, D., Williams, J., Vereecken, L., Lelieveld, J., and Harder, H.: Estimating the atmospheric concentration of Criegee intermediates and their possible interference in a FAGE-LIF instrument, Atmos. Chem. Phys., 17, 7807-7826, https://doi.org/10.5194/acp-17-7807-2017, 2017.

Peltola, J., Seal, P., Inkilä, A., and Eskola, A.: Time-resolved, broadband UV-absorption

spectrometry measurements of Criegee intermediate kinetics using a new photolytic precursor: unimolecular decomposition of CH_2OO and its reaction with formic acid, Phys. Chem. Chem. Phys., 22, 11797-11808, https://doi.org/10.1039/d0cp00302f, 2020.

Raghunath, P., Lee, Y. P., and Lin, M. C.: Computational chemical kinetics for the reaction of Criegee intermediate CH_2OO with HNO_3 and its catalytic conversion to OH and HCO, J. Phys. Chem. A, 121, 3871-3878, https://doi.org/10.1021/acs.jpca.7b02196, 2017.

Sadezky, A., Winterhalter, R., Kanawati, B., Rompp, A., Spengler, B., Mellouki, A., Bras, G. L., Chaimbault, P., and Moortgat, G. K.: Oligomer formation during gas-phase ozonolysis of small alkenes and enol ethers: new evidence for the central role of the Criegee Intermediate as oligomer chain unit, Atmos. Chem. Phys., 8, 2667-2699, https://doi.org/10.5194/acp-8-2667-2008, 2008.

Sakamoto, Y., Inomata, S., and Hirokawa, J.: Oligomerization reaction of the Criegee intermediate leads to secondary organic aerosol formation in ethylene ozonolysis, J. Phys. Chem. A, 117, 12912-12921, https://doi.org/10.1021/jp408672m, 2013.

Sipilä, M., Jokinen, T., Berndt, T., Richters, S., Makkonen, R., Donahue, N. M., Mauldin Iii, R. L., Kurtén, T., Paasonen, P., Sarnela, N., Ehn, M., Junninen, H., Rissanen, M. P., Thornton, J., Stratmann, F., Herrmann, H., Worsnop, D. R., Kulmala, M., Kerminen, V. M., and Petäjä, T.: Reactivity of stabilized Criegee intermediates (sCIs) from isoprene and monoterpene ozonolysis toward SO_2 and organic acids, Atmos. Chem. Phys., 14, 12143-12153, https://doi.org/10.5194/acp-14-12143-2014, 2014.

Taatjes, C. A., Welz, O., Eskola, A. J., Savee, J. D., Scheer, A. M., Shallcross, D. E., Rotavera, B., Lee, E. P. F., Dyke, J. M., Mok, D. K. W., Osborn, D. L., and Percival, C. J.: Direct measurements of conformer-dependent reactivity of the Criegee intermediate CH_3CHOO, Science, 340, 177-180, https://doi.org/10.1126/science.1234689, 2013.

Vereecken, L., Harder, H., and Novelli, A.: The reaction of Criegee intermediates with NO, RO_2, and SO_2, and their fate in the atmosphere, Phys. Chem. Chem. Phys., 14, 14682-14695, https://doi.org/10.1039/c2cp42300f, 2012.

Vereecken, L.: The reaction of Criegee intermediates with acids and enols, Phys. Chem. Chem. Phys., 19, 28630-28640, https://doi.org/10.1039/c7cp05132h, 2017.

Welz, O., Eskola, A. J., Sheps, L., Rotavera, B., Savee, J. D., Scheer, A. M., Osborn, D. L., Lowe, D., Booth, A. M., Xiao, P., Khan, M. A. H., Percival, C. J., Shallcross, D. E., and Taatjes, C. A.: Rate coefficients of C(1) and C(2) Criegee intermediate reactions with formic and acetic Acid near the collision limit: direct kinetics measurements and atmospheric implications, Angew. Chem. Int. Ed., 53, 4547-4550, https://doi.org/10.1002/anie.201400964, 2014.

Welz, O., Savee, J. D., Osborn, D. L., Vasu, S. S., Percival, C. J., Shallcross, D. E., and Taatjes, C. A.: Direct kinetic measurements of Criegee intermediate (CH_2OO) formed by reaction of CH_2I with O_2, Science, 335, 204-207, https://doi.org/10.1126/science.1213229, 2012.

Zhao, Y., Wingen, L. M., Perraud, V., Greaves, J., and Finlayson-Pitts, B. J.: Role of the reaction of stabilized Criegee intermediates with peroxy radicals in particle formation and growth in air, Phys. Chem. Chem. Phys., 17, 12500-12514, https://doi.org/10.1039/c5cp01171j, 2015.